PHYSICAL REVIEW A VOLUME 49, NUMBER 5 MAY 1994

High-order harmonic generation and ionization using ultrashort KrF and Ti:sapphire lasers

K. Kondo, T. Tamida, Y. Nabekawa, and S. Watanabe
Institute for Solid State Physics, University of Tokyo, Roppongi 7-22-1, Minato-ku, Tokyo, 106, Japan
(Received 21 May 1993)

High-order harmonic generation with KrF and Ti:sapphire lasers is analyzed with an emphasis on the contribution of multiply charged ions. It is confirmed that the intensity dependence of strong optical field ionization is explained by the Ammosov-Delone-Krainov (ADK) theory or by the barrier suppression ionization model regardless of the wavelength. The harmonic distributions are compared with the single-atom responses calculated using the short-range potential model with the effective interaction intensity determined by the ADK theory. From this analysis, we propose that for the KrF laser the harmonics above the 21st in Ne and above the 13th in Ar may be due to doubly charged ions.

PACS number(s): 32.80.Rm, 51.70.+f, 42.65.Ky

I. INTRODUCTION

The finding of a plateau in the harmonic distribution [1,2] made it possible to generate coherent soft x rays with a table-top high-power laser. Sarukura *et al.* observed the 25th harmonic (9.9 nm) of a terawatt KrF laser in Ne [3]. Miyazaki and Sakai observed the 41st harmonic (15 nm) of 616 nm in He [4]. Recently, Macklin, Kmetec, and Gordon observed the 109th harmonic (7.4 nm) of a 0.5-TW Ti:sapphire laser in Ne [5], and L'Huillier and Balcou observed the 135th harmonic (7.8 nm) of 1.05 μm in Ne [6]. In these experiments, harmonic radiation was generated in a gaseous target. Akiyama *et al.* observed the 13th harmonic (19.1 nm) of 248 nm in K^+, which was produced in laser plasmas [7]. As for the harmonic plateau, Krause, Schafer, and Kulander showed that the cutoff energy of the plateau was equal to I_p+3U_p, where I_p is the atom (or ion) ionization potential and U_p is the ponderomotive potential [8], given by $U_p=e^2E^2/4m\omega^2$ (e and m are the electron's charge and mass, and E and ω are the field's strength and frequency). This relationship was empirically obtained through calculations of the harmonic spectra using a nonperturbative theory. Recently, Schafer *et al.*, explained the physical meaning of $3U_p$ using a "two-step" semiclassical model for the high field ionization [9]. Corkum also explained $3U_p$ in the same way [10]. He expanded this model to an explanation of multiphoton two-electron ejection from He [11] and the high-energy tail in the above-threshold ionization spectrum [12].

This relationship predicts the low cutoff order for short-wavelength lasers if neutral atoms alone are considered. However, the highest order observed experimentally for KrF lasers was much higher than the cutoff estimated for neutral atoms [1,3,7]. This means that higher-order harmonics for KrF are emitted from multiply charged ions. Krause, Schafer, and Kulander [8] pointed out the contribution of He^+ to the harmonics above the 13th observed by Sarukura *et al.* [3]. Xu, Tang, and Lambropoulos also pointed out the contribution of ions by comparing the harmonic distribution in Ref. [3] with the calculated single-atom response [13]. Obviously, multiply charged ions can emit shorter-wavelength harmonics because they have a larger ionization potential and a higher ionization intensity.

Usually, the numerical calculation of the single-atom response is not so simple when applied to a wide range of experimental conditions, including atom type, laser wavelength, and laser intensity. Becker, Long, and McIver proposed an analytical formula for the single-atom response, including the above-mentioned parameters. They assumed only the continuum and the ground state of a single electron with a three-dimensional δ-function potential [14]. In spite of this simplification, this model has been verified to explain many aspects of harmonic generation [5].

Our previous paper [15] reported experimental results for high-order harmonic generation using KrF and Ti:sapphire lasers. For KrF, self-phase-modulation (SPM) was induced, so higher-order harmonics disappeared with a shorter pulse (100 fs). For Ti:sapphire, the harmonic distribution did not depend on the pulse width of 120–730 fs at a fixed peak intensity. And there was a clear plateau in the harmonic distributions for Ti:sapphire in contrast with those for KrF. If we express the maximum harmonic orders in various rare gases by I_p+kU_p, the values of k are between 1 and 2 for Ti:sapphire, as far as U_p was estimated by the experimental value of the saturation intensity of a neutral atom.

This paper reports on harmonic generation and ionization experiments using KrF (248 nm) and Ti:sapphire (800 and 745 nm) lasers. For KrF, the pulse width was chosen to be 300 fs to prevent SPM in harmonic generation. The experimental results for Ti:sapphire were analyzed in more detail than in our previous study [15]. We analyzed the results of harmonic generation, emphasizing the contributions of multiply charged ions to higher-order harmonics for KrF. The high-field ionization characteristics show the same tendencies for both KrF and Ti:sapphire lasers. The intensity dependences of the ion yield were fitted using Ammosov-Delone-Krainov (ADK) theory [16] and the barrier suppression ionization

(BSI) model [17], which have no wavelength dependence. The harmonic distributions obtained using the KrF and Ti:sapphire lasers were then compared with the single-atom responses calculated using the short-range potential model [14]. In this calculation, the effective intensity was determined by ADK theory in contrast with the previous paper [15], taking into account the inevitable uncertainty in absolute intensity. The calculated harmonic distributions explain many aspects of the rare-gas experiments. Our analysis shows that, using KrF, the harmonics above the 13th in He, between the 11th and 19th in Ne, and between the 9th and 11th in Ar are due to singly charged ions. And we propose that the harmonics above the 21st in Ne and above the 13th in Ar may be due to doubly charged ions.

This paper is organized as follows. The experimental setup and results of harmonic generation are described in Sec. II. Next, the experimental results for strong optical field ionization are analyzed in Sec. III. The analysis was used to provide an intensity calibration for harmonic generation. In Sec. IV the experimental results for harmonic generation are analyzed and discussed. Finally, we summarize this paper in Sec. V.

II. HARMONIC GENERATION

Two kinds of ultrashort lasers were used for harmonic generation in this study. One was a KrF laser whose typical energy and pulse width were 200 mJ and 300 fs, respectively. Details of this laser system are given in Refs. [18] and [19]. The other was a Ti:sapphire laser whose typical energy and pulse width were 33 mJ and 110 fs, respectively. Details of this system are reported in Ref. [20]. The Ti:sapphire laser was operated at either 800 or 745 nm and the KrF laser was operated at 248 nm. The spot sizes were typically 4.5 μm$\times$6.5 μm for KrF when an off-axis parabolic mirror (f: 275 mm) was used and 42 μm in diameter for Ti:sapphire when a planoconvex lens (f: 150 mm) was used.

Figure 1 shows our experimental setup for harmonic generation using KrF. For Ti:sapphire, a planoconvex lens was used instead of the off-axis parabolic mirror, because the pulse-front distortion is neglected for Ti:sapphire. The laser light was focused near the nozzle of a pulsed gas jet. Two types of pulsed gas jet were used. A magnetically driven one was used in the Ti:sapphire experiment and an electrically driven one was used in the KrF experiment. The measured density of the magnetically driven jet was 1.9×10^{18} cm^{-3} at a backing pressure of 7 atm and that of the electrically driven jet was 1.2×10^{18} cm^{-3} at a backing pressure of 9 atm [21]. The generated harmonics went through the 100-μm-wide slit. For KrF, a thin-film filter made of boron was inserted after this slit to cover all harmonics within the dynamic range of the detector. For Ti:sapphire, this filter was not needed because the harmonic distribution has a plateau. When a higher signal level was necessary, the slit was broadened to 500 μm, or eliminated by setting the focal point of the grating just under the nozzle tip. The harmonics were separated by a flat-yield gold-coated grating, which covered the shorter-wavelength region (5–40 nm). For the longer-wavelength region (25–250 nm), a 0.2-m focal-length monochromator (λ-Minuteman Model 302-VM) was used by modifying it to use a microchannel plate (MCP). The separated harmonics were detected by a two-stage MCP (Hamamatsu Model F3490-21px). The spectrum image on the MCP phosphorous screen was captured by a silicon intensifier target (SIT) camera. The image data were analyzed using a frame memory (Hamamatsu Model C1330). The frame memory is a two-dimensional image analyzer. The absolute photon

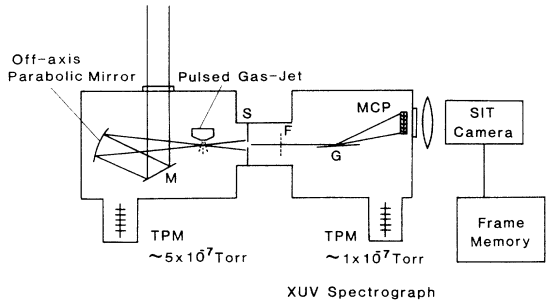

FIG. 1. Experimental setup for harmonic generation using a KrF laser. TPM means a turbomolecular pump.

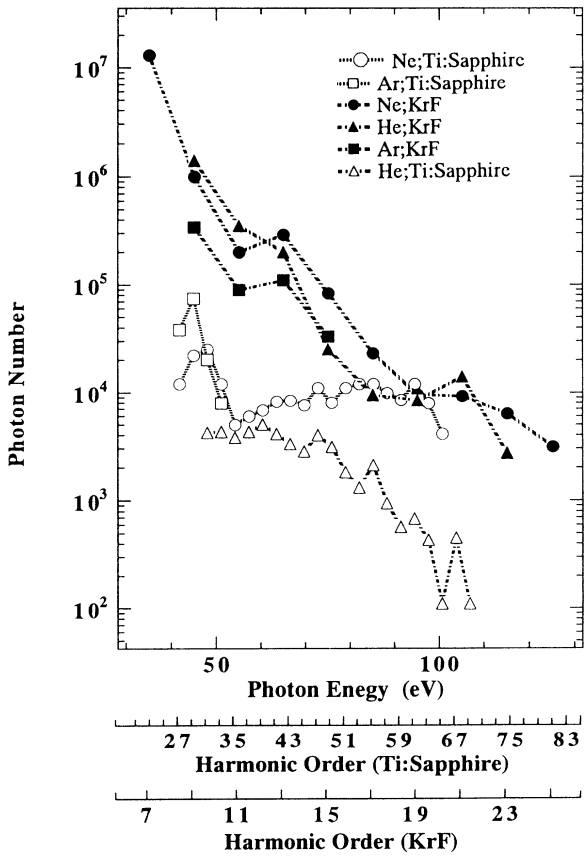

FIG. 2. Harmonic distributions above 35 eV for various target gases using KrF and Ti:sapphire lasers. KrF data were taken from Ref. [3]. In Ti:sapphire, the peak intensities are 3.2×10^{15} W/cm^2 for He, 3.1×10^{15} W/cm^2 for Ne, and 3.3×10^{15} W/cm^2 for Ar. Gas densities are 1.9×10^{18} cm^{-3} for Ti:sapphire and 1.2×10^{18} cm^{-3} for KrF.

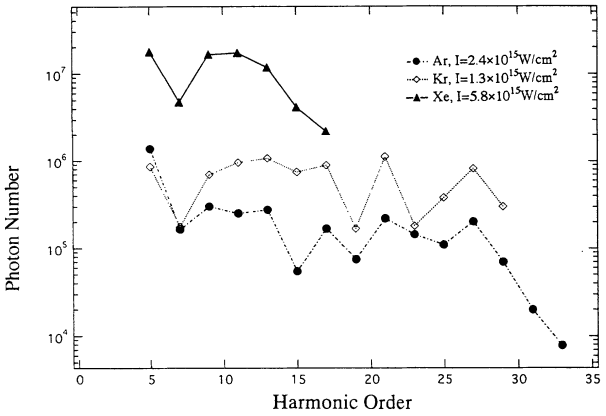

FIG. 3. Harmonic distributions below 55 eV for various target gases using a Ti:sapphire laser. The peak intensities are 5.8×10^{14} W/cm^2 for Xe, 1.3×10^{15} W/cm^2 for Kr, and 2.4×10^{15} W/cm^2 for Ar.

number was estimated by measuring the 7th-harmonic intensity for KrF with a high-speed MCP (Hamamatsu Model F3654-21s). The setup for this experiment is also described in Refs. [3] and [15].

The harmonic distributions for Ti:sapphire and KrF in the shorter-wavelength region are summarized in Fig. 2, which shows a clear plateau up to the 65th harmonic in Ne and up to the 69th in He for Ti:sapphire. However, the harmonic distribution gradually decreases to the 25th harmonic in Ne and to the 23rd in He for KrF with some recoveries. In the lower orders, much more harmonic intensity was detected using KrF than using Ti:sapphire, while it was almost equal in the higher orders. The harmonic distributions for Ti:sapphire in the longer-wavelength region are shown in Fig. 3. The absolute photon numbers are slightly corrected to those at a gas density of 1.9×10^{18} cm^{-3}, assuming N^2 dependence. The maximum harmonic orders observed using Ti:sapphire were 17th for Xe, 29th for Kr, 33rd for Ar, 71st for Ne, and 69th for He.

These maximum orders were far below the cutoff-order relation of I_p+3U_p even for Ti:sapphire when the saturation intensity obtained in experiment was used. Usually an uncertainty factor of 2 would be inevitable to determine the absolute intensity. Therefore, we introduce the "effective intensity" in the next section by calibrating the absolute intensity using the comparison between ionization experiments and theories.

III. MEASUREMENT AND ANALYSIS OF IONIZATION

The effective interaction intensity, where emitting atoms or ions can interact before ionizing to the next charge state, determines the cutoff order of the harmonic plateau. Therefore, the ionization dynamics must be examined to understand the mechanism of high-order harmonic generation. We measured the ion yield for each charge state by varying the peak intensity with a time-of-flight analyzer (R. M. Jordan Company). A target gas (He, Ne, Ar, Kr, or Xe) backfilled the target chamber to a pressure of 3×10^{-6} Torr for all gases in Ti:sapphire and for He in KrF. Except for He, the backing pressure was 4.7×10^{-7} Torr for KrF. A turbomolecular pump was used to evacuate the chamber to below 5×10^{-9} Torr. The acceleration field was 900 V/cm and the field-free drift length was 1.4 m. The ions were detected with a two-stage MCP, which has a total gain of approximately 10^6. The time resolution was good enough to resolve H_2^+ from He^{2+}. The ion spectra were recorded with a digital signal analyzer (Tektronix DSA 602). The laser beam was focused by an achromatic lens for KrF and a planoconvex lens for Ti:sapphire. The focal lengths were 300 and 150 mm, respectively.

For KrF, the scattered light and the spectrum of H_2O-related ions (H^+, H_2^+, O^{2+}, and H_2O^+) are too strong. Therefore, the signals of the relevant rare-gas ions are suppressed because of the MCP saturation. Thus a gate voltage of 800 V, with a 1-μs duration, was applied to one stage of the MCP. An appropriate delay selected the charge states of the rare gases.

In general, ionization under an intense laser field is divided into two regimes, multiphoton and tunneling. These two regimes are usually distinguished by the Keldysh parameter $\gamma=(I_p/2U_p)^{0.5}$, where the multiphoton

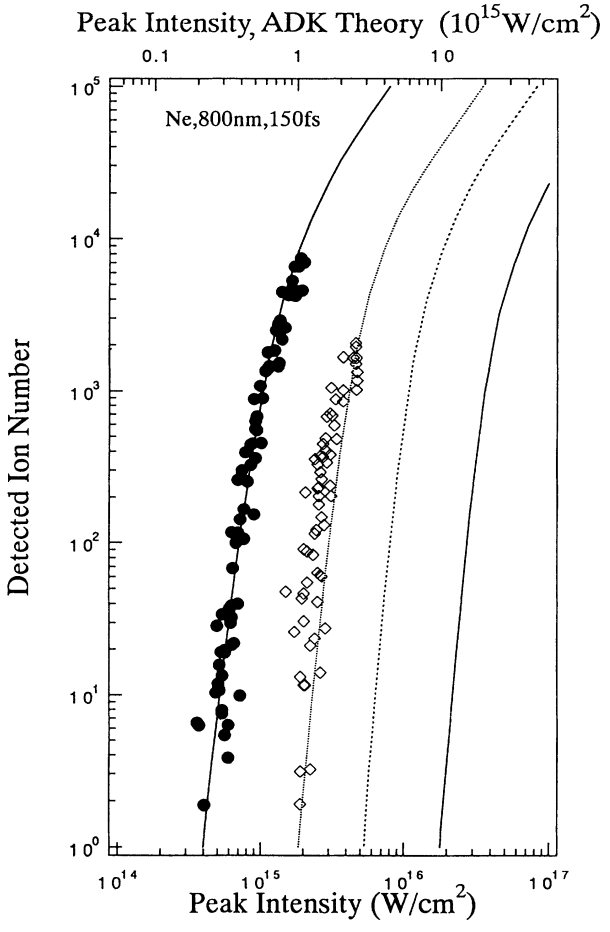

FIG. 4. Ne ion-production rate as a function of peak intensity using a Ti:sapphire laser (800 nm). Theoretical curves are from ADK theory. The upper and lower horizontal axes show the intensity fitted to ADK theory and the raw experimental values, respectively. The shift between them has a factor of 1.8.

regime corresponds to $\gamma \gg 1$ and the tunneling regime to $\gamma \ll 1$, although the full range of γ is covered by the Keldysh theory [22]. Therefore, ionization by a Ti:sapphire laser is thought to be within the tunneling region. For example, $\gamma = 0.45$ for a neutral Ne at 8.8×10^{14} W/cm^2 using Ti:sapphire. However, using KrF, U_p is one-tenth that using Ti:sapphire at the same intensity. In fact, $\gamma = 1.4$ for neutral Ne at 8.8×10^{14} W/cm^2 for KrF. Thus ionization by a KrF laser is usually classified into the multiphoton region. Recently, for the picosecond or subpicosecond regimes, the tunneling theories, or more extremely the BSI model, have been verified [17,23] to explain well the appearance intensities for $\gamma > 1$. Gibson, Luk, and Rhodes compared the appearance intensity for a subpicosecond KrF laser using various ionization models [23], for the range from $\gamma = 1$ to 8. They showed that ADK theory gave uniformly better quantitative agreement over the entire range of gases and charge states.

To understand the ionization mechanism in this experiment, we also compared the experimental results for various rare gases at the wavelengths of Ti:sapphire and KrF lasers using the BSI model [17], ADK theory [16], Keldysh-Faisal-Reise (KFR) theory [24], and the modified KFR theory [25]. Typical intensity dependences of ionization are shown in Figs. 4–6. Figure 4 is for Ne using Ti:sapphire (800 nm). Figures 5 and 6 are for Ne and Ar, respectively, using KrF (248 nm). The peak intensity was estimated using $I_{\text{peak}} = 0.61E/(\tau \pi r^2)$, where E is the laser energy, τ is the pulse width (full width at half maximum), and r is the spot radius (half width at half maximum). In Figs. 5(a) and 6(a), the experimental results are compared using the BSI model. In this comparison, there is no intensity shift between them. Thus this model gives the correct appearance intensity for the singly charged state. However, this model predicts a rather narrow separation between each ionization curve. In Figs. 4, 5(b), and 6(b), the experimental results are compared using ADK theory. All the experimental curves fit the ADK theory better than the BSI model. The upper and lower horizontal axes show the intensity fit to ADK theory and measured intensity, respectively. The intensity shifts that give the best fits are a factor of 1.8 in Fig. 4 and a factor of 2 in Figs. 5(b) and 6(b). This overestimation of the measured intensity comes from the incompleteness and/or the underestimation of the focal spot size. The full measured energy does not concentrate on the central Gaussian profile. Usually an uncertainty factor of 2 would be inevitable in determining the absolute intensity. Slight deviations from the theory for Ne^{2+} and Ne^{3+} at 248 nm are observed at higher intensities.

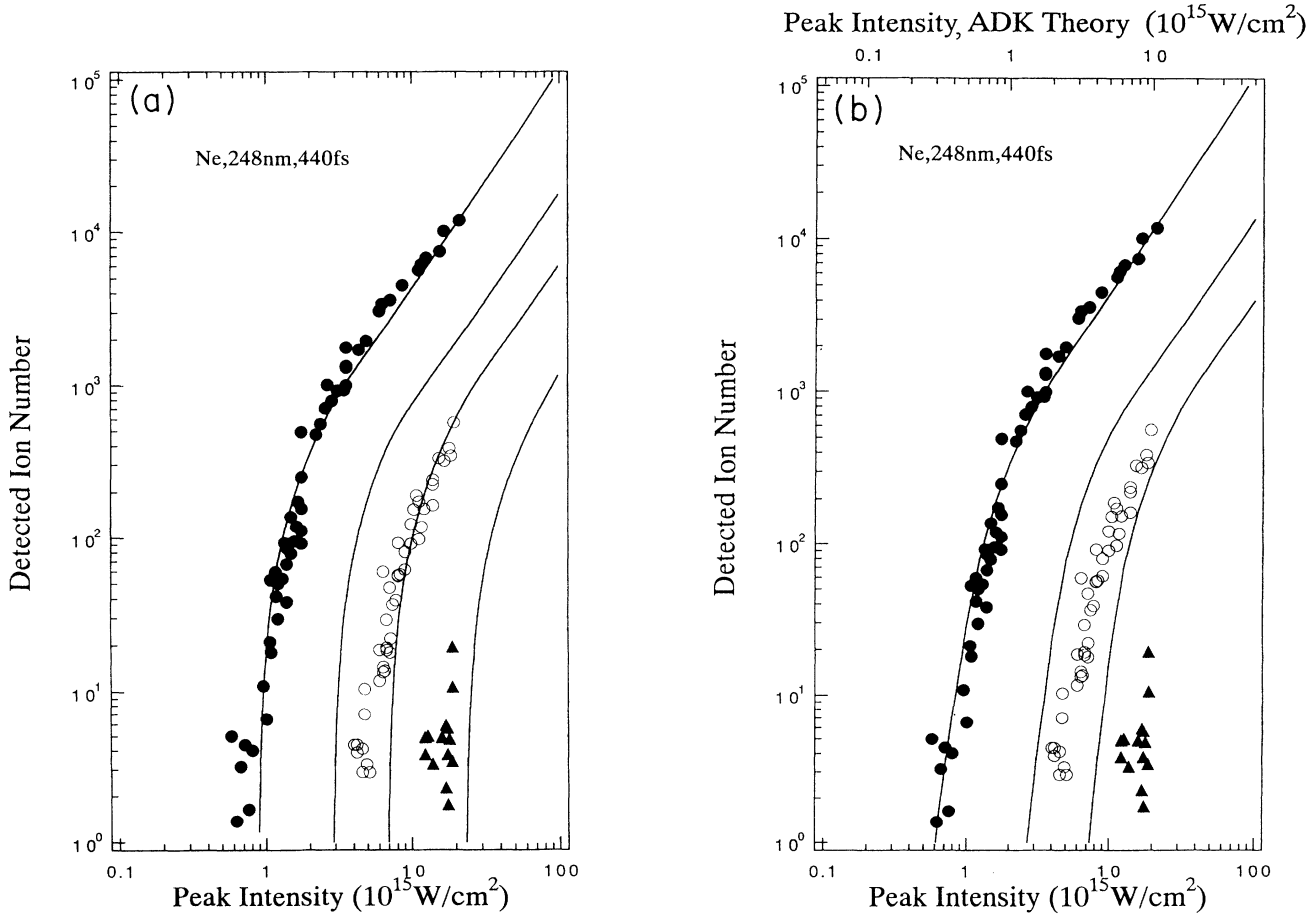

FIG. 5. Ne ion-production rate as a function of peak intensity using a KrF laser (248 nm). Experimental results are compared using the BSI model and ADK theory. (a) Theoretical curves from the BSI model. There is no intensity shift between theory and experiment. (b) Theoretical curves from ADK theory. The intensity shift has a factor of 2.

The reason for this is not clear, but could be due to the expanding spot size and/or beam breakup. For Ar, ADK theory predicts quite well up to Ar^{4+}. The Ar^{5+} signal is mixed with that of O^{2+} and therefore raised. The intensity dependence of high field ionization for He can be also explained by ADK theory and the BSI model, although the enhancement of He^{2+} due to two-electron ejection was observed using Ti:sapphire (745 nm), but not in KrF. The details are reported in Ref. [26]. The KRF theory does not give the correct separation and the modified KRF theory needs an anomalous shift (factor of 8) in the intensity. Throughout the experiments, there was no wavelength dependence, which is the feature of the BSI model and ADK theory. The question is now what is the basic mechanism of ionization. In the regime of a very short pulse at a high intensity, BSI seems more probable than the multiphoton scheme. The Coulomb barrier of the atom is suppressed so fast that an electron can be released from the atom within the laser duration, whereas the laser duration is too short to ionize an atom in the multiphoton regime. In the BSI model, the time for tunneling through the Coulomb barrier is zero above the threshold intensity. Therefore, the BSI model is thought to give the limit of tunneling ionization at a high intensity. Unfortunately the BSI model, which includes only the ionization potential and the ionic charge, is too simple to explain the details of ionization. In contrast to this, ADK theory takes into account the effect of tunneling around the appearance intensity and the wave function of the ion core in each ionization stage. Actually, ADK theory can explain the intensity dependence around the appearance intensity and the separation of curves for each charge state better than the BSI model, although an appropriate intensity shift is necessary for fitting with experimental results.

As the result of these discussions, we selected ADK theory to explain the high field ionization by a subpicosecond laser pulse and used the intensity corrected by ADK theory in the following analysis, rather than the raw experimental value.

IV. ANALYSIS OF HARMONIC DISTRIBUTION

The harmonic distributions are determined mainly by peak intensity for a given confocal parameter and atom when peak intensity is below the ionization level. The intensity of each harmonic is calculated by the spatial and temporal integration of the atomic response combined with propagation and phase-matching effects [27]. When peak intensity is well above the ionization level, as in Ref.

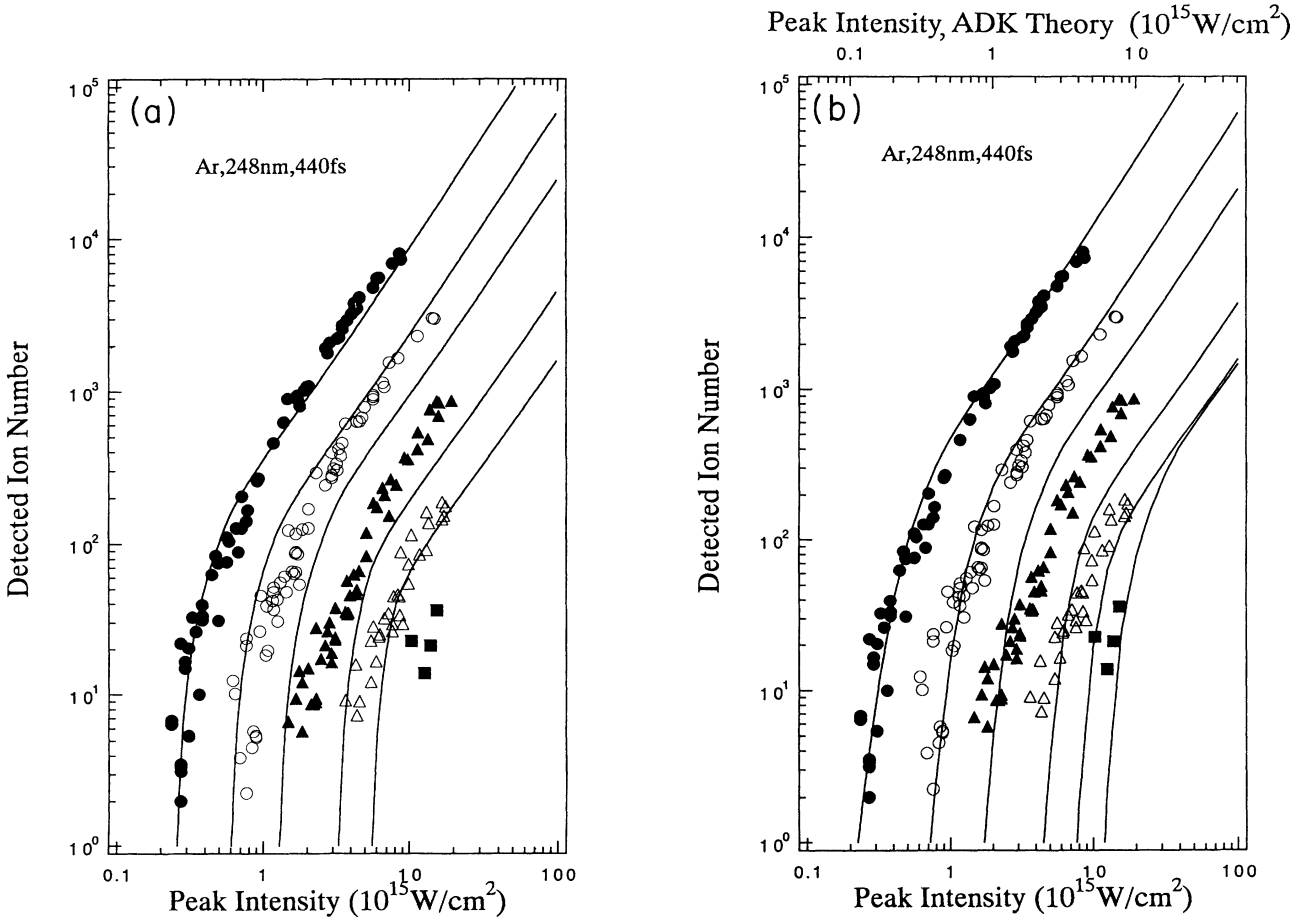

FIG. 6. Ar ion-production rate as a function of peak intensity using a KrF laser (248 nm). Experimental results are compared with the BSI model and ADK theory. (a) Theoretical curves from the BSI model. There is no intensity shift between theory and experiment. (b) Theoretical curves from ADK theory. The intensity shift has a factor of 2.

[3], however, the calculation is complicated because successive charge states occur and the phase mismatch due to free electrons is added. In the plateau region, the shape of the harmonic distribution is determined by the atomic response [27], although the absolute photon number is affected by phase matching. Our previous paper [15] described that the phase mismatch was dominated by free electrons assuming full ionization. That description should be corrected because harmonics are generated a long time before full ionization. This paper calculated the single-atom responses $[|d(q\omega)|^2]$ using the effective intensities (I_{eff}) of each charge state, instead of spatial and temporal integration. This simplification means that the temporal and spatial regions above I_{eff} both contribute in the same way to the harmonic distribution.

The dynamics of Ne charge states within a pulse at the center of the focal spot are calculated using ADK theory for a peak intensity of 1.72×10^{15} W/cm^2 using Ti:sapphire in Fig. 7. The ionization rates for 3% and 50% ionization of a neutral atom correspond to 4×10^{12} and 6×10^{13} s^{-1}, respectively. Of course, the relationship between the percentage of ionization and the ionization rate depends on the pulse width and the peak intensity.

In order to calculate the single-atom response using the short-range potential model, the effective interaction intensity must be determined. The question is now how to estimate the effective intensity. We determined the effective intensities by the fits to all of the experimental data for Ti:sapphire and KrF taking into account the maximum harmonic orders and relative heights among rare gases. The effective intensity can be defined by both the instantaneous ionization rate, which does not depend on the pulse width or the peak intensity, and by the integrated fraction of ionization. This paper used the fraction of ionization at the center of the focal spot, because it can be compared with the experiment. Of course, the effective intensities should correspond to the same ionization level among rare gases. In Fig. 8, the harmonic distributions of all rare gases for Ti:sapphire are compared with those calculated using the short-range potential

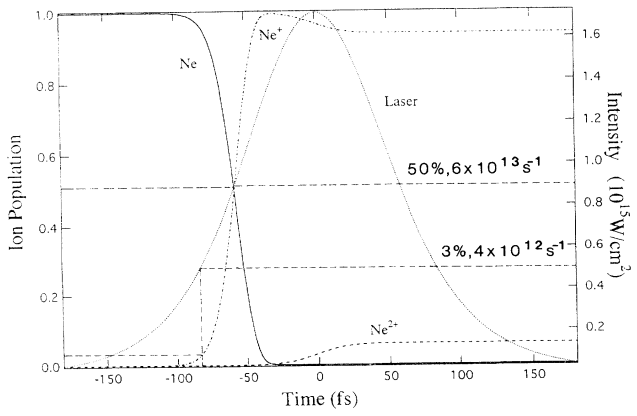

FIG. 7. Calculation of ion dynamics in Ne using ADK theory. The peak intensity is 1.72×10^{15} W/cm^2, with a pulse width of 120 fs. Neutral Ne atoms are ionized at a 3% level at an intensity of 5×10^{14} W/cm^2 and at a 50% level at an intensity of 9×10^{14} W/cm^2.

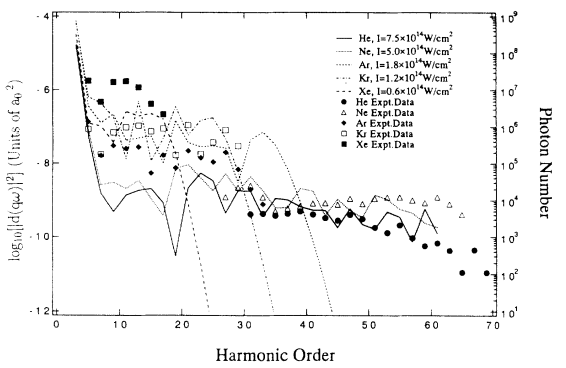

FIG. 8. Harmonic distributions for all rare gases using a Ti:sapphire laser compared with the single-atom responses $|d(q\omega)|^2$, which were calculated using the short-range potential model. For all gases, the effective intensities are estimated to be 3% ionization of neutral atoms.

model. The experimental plots were taken from Figs. 2 and 3, which overlap at the 27th harmonic in Ar as observed by both spectrometers. As a result, the estimated interaction intensity corresponded to 3% ionization. The calculation explains fairly well the cutoff orders and relative height of the plateau among rare gases, although orders above the 61st were not calculated for He or Ne. The cutoff orders from I_p+3U_p were the 101st and 71st for He and Ne, respectively. As mentioned later, this effective intensity also gives a good fit to the experiment using KrF.

This effective intensity should be compared with other studies. For He, Krause, Schafer, and Kulander estimated the harmonic spectra at the intensity that produced an ionization rate of $\sim2\times10^{12}$ s^{-1}, which corresponds to $\sim6\times10^{14}$ W/cm^2 at 800 nm and 4×10^{14} W/cm^2 at 248 nm [8]. The effective intensity in the present paper was 7.5×10^{14} W/cm^2 regardless of the wavelength, corresponding to an ionization rate of 3×10^{12} s^{-1}. For He$^+$ in KrF, the effective intensity in this paper (4.8×10^{15} W/cm^2) is comparable with 4.4×10^{15} W/cm^2 estimated from the ionization rate of 3×10^{12} s^{-1} [8] and with 5.5×10^{15} W/cm^2 [13]. Our estimates agree reasonably well with other studies for He. For Ne using Ti:sapphire, Macklin, Kmetec, and Gordon observed the fractional ionization from the blueshift of the fundamental spectrum [5]. At the effective intensity in the present paper (5×10^{14} W/cm^2), the measured fractional ionization of Ref. [5] was 2%, in good agreement with a 3% ionization level. But they estimated an ionization rate of $\sim7\times10^{12}$ s^{-1} from the I^5 law and observed 30–40 % ionization at 10^{15} W/cm^2. At this intensity, our calculation gives 10^{14} s^{-1} and 70% ionization. The reason for these discrepancies is not clear. As a whole, the validity and physical meaning of a 3% ionization level is still unclear and should be open to discussion.

In harmonic generation using a KrF laser, the peak intensity is above 10^{17} W/cm^2. Figure 9 shows the dynamics of the Ne charged state at an earlier stage of the laser pulse for a peak intensity of 4×10^{17} W/cm^2 with a 300-fs pulse. The neutral Ne has already vanished 600 fs before

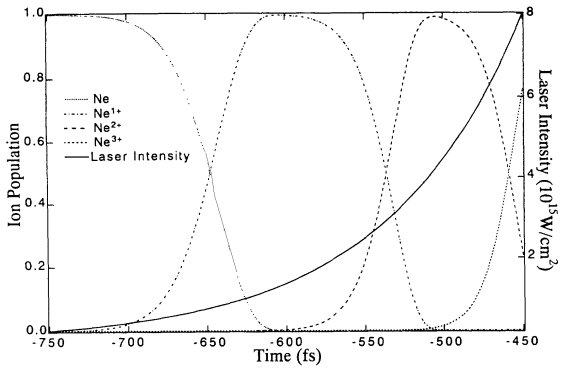

FIG. 9. Calculation of ion dynamics in Ne using ADK theory. The peak intensity is 4×10^{17} W/cm^2, with a pulse width of 300 fs. Dynamics are shown only at an early stage of the laser pulse (from $t=-750$ to -450 fs; $t=0$ fs corresponds to the laser peak).

the laser peak. Various charge states appear and vanish one after another up to the 8th charge state, which appears 130 fs before the peak. Therefore, the high-order harmonics for a KrF laser are probably emitted from multiply charged ions.

Xu, Tang, and Lambropoulos [13] have pointed out the contribution of ions to our experiment in Ref. [3], as shown in Fig. 10. Krause, Schafer, and Kulander also pointed out this contribution [8]. Higher-order harmonics for He using KrF were attributed to the singly charged ion. In Fig. 10, curves calculated from the short-range potential model are shown for He and He^+, along with the calculation of Ref. [13]. The intensities in Ref. [13] were used for the calculation. Both calculations clearly explain the contribution of the ion, although there are some differences in the detailed shapes. This comparison shows the range of validity for the short-range potential model. In Ref. [13], the intensities of 6×10^{14} W/cm^2 for He and 5.5×10^{15} W/cm^2 for He^+ were used to explain the harmonic distribution of KrF.

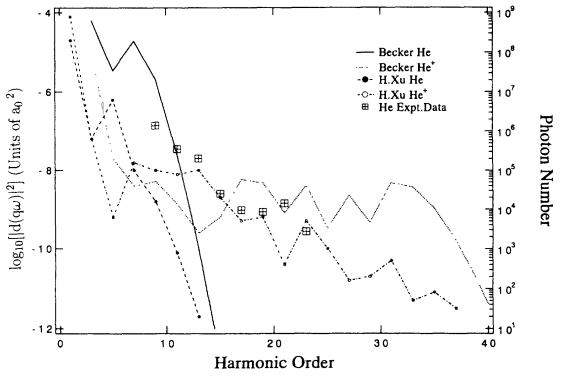

FIG. 10. Comparison between the calculated single-atom response using the short-range potential model and the numerical calculation by Xu, Tang, and Lambropoulos [13] for He and He^+ using a KrF laser. The effective intensities are 6.0×10^{14} W/cm^2 for He and 5.5×10^{15} W/cm^2 for He^+. Experimental plots are also shown using squares.

These values are almost the same as our effective intensities of 7.0×10^{14} and 4.8×10^{15} W/cm^2.

In Fig. 11(a), the experimental data are compared with the short-range potential model for Ne using KrF. The effective intensity for successive charge states was also determined by ADK theory. The recovery at the 13th and 21st harmonics can be explained by the contributions of Ne^+ and Ne^{2+}, respectively. Of course, the uncertainty in effective intensity should also be considered. Figure 11(b) tries to explain the harmonic distributions in Ne in terms of Ne^+ at the double intensity (3.5×10^{15} W/cm^2), which corresponds to 50% ionization, and is very close to the appearance intensity of Ne^{2+} as shown in Fig. 5(b). Above the 11th harmonic, the double intensity for Ne^+ might explain the distribution only with the weight of 0.1 or 0.01 for Ne^+ relative to Ne. We think that it would be natural to take our effective intensity and to attribute the harmonics above the 21st to doubly charged neon.

The contribution of Ar^{2+} is more probable than that of Ne^{2+}, as shown in Fig. 12(a). In Fig. 12(b) the calculated harmonic distributions for Ar^+ at the double intensity (9.2×10^{14} W/cm^2) are shown with the weights of 1, 0.1, and 0.01. Even the double intensity cannot explain the 15th harmonic. This is verified by the ionization experi-

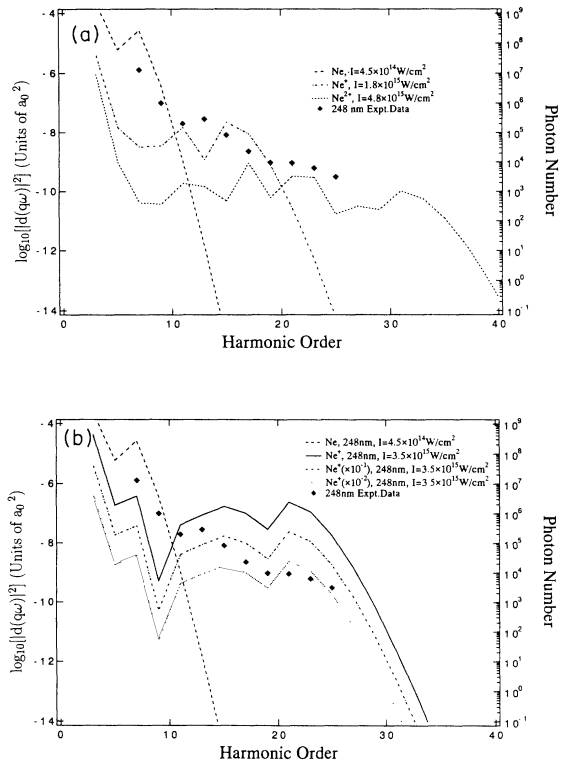

FIG. 11. Comparison between the observed harmonic distribution of Ne using a KrF laser and the single-atom responses of Ne, Ne^+, and Ne^{2+} calculated using the short-range potential model. (a) The effective intensities are 4.5×10^{14} W/cm^2 for Ne, 1.8×10^{15} W/cm^2 for Ne^+, and 4.8×10^{15} W/cm^2 for Ne^{2+}. All of the effective intensities are determined at 3% ionization for each charge state. All of the curves are superposed with an equal weight. (b) The effective intensity is double (3.5×10^{15} W/cm^2) the 3% ionization for Ne^+. Calculated curves of Ne^+ are shown with the weights of 1, 0.1, and 0.01 relative to Ne.

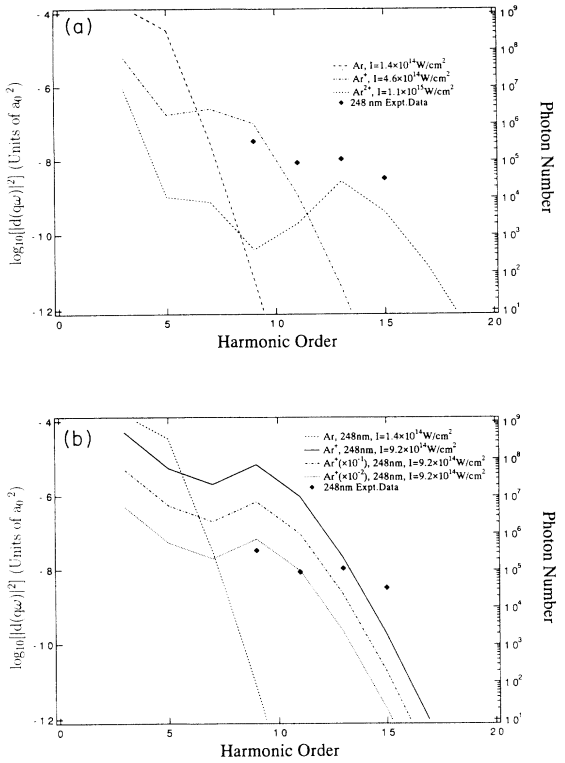

FIG. 12. Comparison between the observed harmonic distribution of Ar using a KrF laser and the single-atom responses of Ar, Ar^+, and Ar^{2+} calculated using the short-range potential model. (a) The effective intensities are 1.4×10^{14} W/cm^2 for Ar, 4.6×10^{14} W/cm^2 for Ar^+, and 1.1×10^{15} W/cm^2 for Ar^{2+}. All of the effective intensities are determined at 3% ionization for each charge state. All of the curves are superposed with an equal weight. (b) The effective intensity is double (9.2×10^{14} W/cm^2) the 3% ionization for Ar^+. Calculated curves of Ar^+ are shown with the weights of 1, 0.1, and 0.01 relative to Ar.

ment results shown in Fig. 6. At 9.2×10^{14} W/cm^2, no Ar^+ remains in the central region at the focal point, either in ADK theory or in the experiment, because Ar^{2+} has already appeared. Note that the relationship between the atomic response and the absolute photon number is conserved among Figs. 10–12. These figures therefore explain fairly well the relative harmonic intensity among He, Ne, and Ar.

In the above analysis, the contribution of the singly charged state of He is clear because the doubly charged state has no electron. The question is the contribution of the doubly charged states of Ne and Ar. Calculated and experimental harmonic spectra often show strange features (anomalous peaks and/or recoveries) in a plateau region. Whether the second recovery in Ne comes from a plateau region or from after the cutoff of a single charge state is still debatable.

The 3% ionization level is of course empirical and does not have much physical meaning. The ionization level at a given intensity depends strongly on the ionization model. Therefore, it is quite unclear how many atoms or ions survive at the effective intensity for harmonic generation. Furthermore the short-range potential model is not a perfect theory for explaining the experiment. To discuss the experimental results in more detail, it is necessary to perform a computer simulation for solving a time-dependent Schrödinger equation.

To obtain higher-order harmonics, we need to use ions with a larger ionization potential at higher laser intensities. This would be possible with double-pulse excitation, where the first pulse is used for ionizing an atom to the desired charge state and the second pulse is used for generating harmonics. For example, the ionization potentials are 125 and 223 eV for Ne^{3+} and Ne^{4+}, respectively. If these ions are exposed to an intensity above 5×10^{15} and 2×10^{16} W/cm^2, respectively, which is the 3% ionization level for each ion, cutoff orders up to the 41st and 113th harmonics would be possible, although the harmonic intensity would be low.

V. SUMMARY

Multiply charged ions may play an important role in harmonic generation using an ultrashort KrF laser, while only the neutral atoms contribute for a Ti:sapphire laser. There is some recovery and/or inversion along the harmonic order for the KrF harmonic distributions. The intensity dependence of the ion yields can be explained by ADK theory, with an intensity shift of around 2, regardless of the wavelength.

We calculated the dynamics of successive charge states using ADK theory. The short-range potential model, with effective intensities for each charge state, explains the harmonic distributions obtained using both Ti:sapphire and KrF, where ADK theory is assumed.

ACKNOWLEDGMENTS

The helpful discussions with N. Sarukura and K. Sajiki are acknowledged. We also thank A. Sagisaka for his technical assistance.

[1] A. McPherson, G. Gibson, H. Jara, U. Johann, T. S. Luk, I. A. McIntyre, K. Boyer, and C. K. Rhodes, J. Opt. Soc. Am. B **4**, 595 (1987).
[2] M. Ferray, A. L'Huillier, X. F. Li, L. A. Lompre, G. Mainfray, and C. Manus, J. Phys. B **21**, L31 (1988).
[3] N. Sarukura, K. Hata, T. Adachi, R. Nodomi, M. Watanabe, and S. Watanabe, Phys. Rev. A **43**, 1669 (1991).
[4] K. Miyazaki and H. Sakai, J. Phys. B **25**, L83 (1992).
[5] J. J. Macklin, J. D. Kmetec, and C. L. Gordon III, Phys. Rev. Lett. **70**, 774 (1993).
[6] A. L'Huillier and Ph. Balcou, Phys. Rev. Lett. **70**, 774 (1993).
[7] Y. Akiyama, K. Midorikawa, Y. Matsunami, Y. Nagata, M. Obara, H. Tashiro, and K. Toyoda, Phys. Rev. Lett. **69**, 2176 (1992). Afterwards, the 21st harmonic was observed in Pb ions.
[8] J. L. Krause, K. J. Schafer, and K. C. Kulander, Phys. Rev. Lett. **68**, 3535 (1992).
[9] K. J. Schafer, B. Yang, L. F. DiMauro, and K. C. Kulander, Phys. Rev. Lett. **70**, 1599 (1993).

[10] P. B. Corkum, Phys. Rev. Lett. **71**, 1994 (1993).
[11] D. N. Fittinghoff, P. B. Bolton, B. Chang, and K. C. Kulander, Phys. Rev. Lett. **69**, 2642 (1992).
[12] U. Mohideen, M. H. Sher, H. W. K. Tom, G. D. Aumiller, O. R. Wood II, R. R. Freeman, J. Bokor, and P. H. Bucksbaum, Phys. Rev. Lett. **71**, 509 (1993).
[13] H. Xu, T. Tang, and P. Lambropoulos, Phys. Rev. A **46**, R2225 (1992).
[14] W. Becker, S. Long, and J. K. McIver, Phys. Rev. A **41**, 4112 (1990).
[15] K. Kondo, N. Sarukura, K. Sajiki, and S. Watanabe, Phys. Rev. A **47**, R2480 (1993).
[16] V. Ammosov, N. B. Delone, and V. P. Krainov, Zh. Eksp. Teor. Fiz. **64**, 1191 (1986) [Sov. Phys. JETP **64**, 1191 (1986)].
[17] S. Augst, D. Strickland, D. D. Meyerhofer, S. L. Chin, and J. H. Eberly, Phys. Rev. Lett. **63**, 2212 (1989); S. Augst, D. D. Meyerhofer, D. Strickland, and S. L. Chin, J. Opt. Soc. Am. B **8**, 858 (1991).
[18] M. Watanabe, K. Hata, T. Adachi, R. Nodomi, and S. Watanabe, Opt. Lett. **15**, 845 (1990).
[19] M. Mizoguchi, K. Kondo, and S. Watanabe, J. Opt. Soc. Am. B **9**, 560 (1992).
[20] Y. Nabekawa, N. Sarukura, K. Sajiki, K. Kondo, and S. Watanabe, Opt. Lett. **18**, 1922 (1993).
[21] T. Adachi, K. Kondo, and S. Watanabe, Appl. Phys. B **55**, 323 (1992).
[22] L. V. Keldysh, Zh. Eksp. Teor. Fiz. **47**, 1945 (1964) [Sov. Phys. JETP **20**, 1307 (1965)].
[23] G. Gibson, T. S. Luk, and C. K. Rhodes, Phys. Rev. A **41**, 5049 (1990).
[24] H. R. Reiss, Phys. Rev. A **22**, 1786 (1980).
[25] M. D. Perry, A. Szoke, O. L. Landen, and E. M. Campbell, Phys. Rev. Lett. **60**, 1270 (1988).
[26] K. Kondo, A. Sagisaka, T. Tamida, Y. Nabekawa, and S. Watanabe, Phys. Rev. A **48**, R2531 (1993).
[27] A. L'Huillier, Ph. Balcou, S. Candel, K. J. Schafer, and K. C. Kulander, Phys. Rev. A **46**, 2778 (1992).